




Effect of triple-tail surfactant on the morphological properties of polyethersulfone-based membrane and its antifouling ability

Rosmanisah Mohamat^{1,2}, Suriani Abu Bakar^{1,2,*} , Muqoyyanah^{1,3}, Azmi Mohamed^{1,4}, Siti Nur Elida Aqmar Mohamad Kamal⁵, Mohd Hafiz Dzarfan Othman⁵, Rosiah Rohani⁶, Mohamad Hafiz Mamat⁷, Mohd Khairul Ahmad⁸, Hamdan Hadi Kusuma⁹, and Budi Astuti¹⁰

¹ Nanotechnology Research Centre, Faculty of Science and Mathematics, Universiti Pendidikan Sultan Idris, 35900 Tanjung Malim, Perak, Malaysia

² Department of Physics, Faculty of Science and Mathematics, Universiti Pendidikan Sultan Idris, 35900 Tanjung Malim, Perak, Malaysia

³ Research Center for Advanced Materials, National Research and Innovation Agency (BRIN), 15314 South Tangerang, Banten, Indonesia

⁴ Department of Chemistry, Faculty of Science and Mathematics, Universiti Pendidikan Sultan Idris, 35900 Tanjung Malim, Perak, Malaysia

⁵ Advanced Membrane Technology Research Centre (AMTEC), Universiti Teknologi Malaysia, 81310 Skudai, Johor, Malaysia

⁶ Department of Chemical and Process Engineering, Faculty of Engineering and Built Environment, Universiti Kebangsaan Malaysia (UKM), 43600 Bangi, Selangor, Malaysia

⁷ NANO-ElecTronic Centre (NET), Faculty of Electrical Engineering, Universiti Teknologi MARA (UiTM), 40450 Shah Alam, Selangor, Malaysia

⁸ Microelectronic and Nanotechnology—Shamsuddin Research Centre (MiNT-SRC), Faculty of Electrical and Electronic Engineering, Universiti Tun Hussein Onn Malaysia, Parit Raja, 86400 Batu Pahat, Johor, Malaysia

⁹ Physics Department, Faculty of Sciences and Technology, Universitas Islam Negeri Walisongo Semarang, Semarang, Central Java, Indonesia

¹⁰ Physics Department, Faculty of Mathematics and Natural Science, Universitas Negeri Semarang, Semarang, Indonesia

Received: 13 June 2022

Accepted: 14 August 2022

© The Author(s), under exclusive licence to Springer Science+Business Media, LLC, part of Springer Nature 2022

ABSTRACT

This study presents a simpler approach to directly synthesize graphene oxide (GO) via electrochemical exfoliation method utilizing customized triple-tail 1-butyl-3-methyl-imidazolium, 1, 4-bis(neopentyloxy)-3-(neopentylcarbonyl)-1, 4-dioxobutane-2-sulfonate (BMIM-TC14) and sodium 1,4-bis(neopentyloxy)-3-(neopentylcarbonyl)-1,4-dioxobutane-2-sulfonate (TC14) surfactants. The synthesized GO and titanium dioxide (TiO₂) were then used as additives in the fabrication of polyethersulfone (PES)-based nanofiltration (NF) membrane via non-solvent-induced phase separation method. The dye rejection

Handling Editor: Dale Huber.

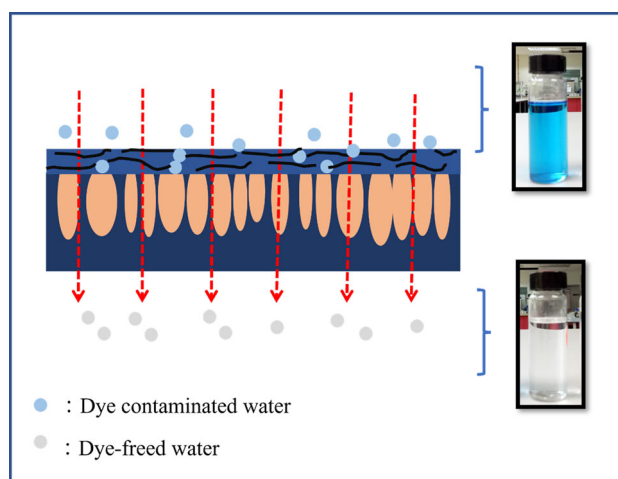
Address correspondence to E-mail: absuriani@yahoo.com

<https://doi.org/10.1007/s10853-022-07646-2>

Published online: 30 August 2022

performance and antifouling ability of the fabricated PES/ $\text{GO}_{\text{BMIM-TC14}}/\text{TiO}_2$ and PES/ $\text{GO}_{\text{TC14}}/\text{TiO}_2$ NF membranes were then investigated by comparing it with pristine PES membrane. It is worth noting that the utilization of triple-tail surfactant obviously enhanced membrane's morphology in which PES/ $\text{GO}_{\text{TC14}}/\text{TiO}_2$ NF membrane showed the highest hydrophilicity as shown by its lowest contact angle (68.98°). According to dead-end cell measurement, higher pure water flux ($200.265 \text{ L/m}^2\cdot\text{h}$) and dye rejection (86.58%) were also obtained by PES/ $\text{GO}_{\text{TC14}}/\text{TiO}_2$ NF membrane compared to other fabricated membranes. Higher GO amount in the sample resulted from the utilization of triple-tail surfactants that was believed to improve the dye rejection performance and antifouling abilities. Both GO-based NF membranes also showed a high flux recovery ratio ($> 100\%$) compared to the pristine PES membrane (5.88%), thereby implied their excellent antifouling ability.

GRAPHICAL ABSTRACT



Introduction

Over the past years, textile industries development has led to a major problem of water pollution since a huge amount of waste from these industries has been released directly into the water. The presence of organic dyes in the wastewater effluents can cause severe problems since they are toxic, carcinogenic and dangerous to human health [1]. In this kind of situation, there is an urgent need to expand some technologies that are led to eliminate the environment pollutant, low cost and eco-friendly. Membrane separation has grown exponentially to remove dye

contamination and becomes the most preferred method to treat wastewater due to their merits of removing a wide range of contaminants, high efficient, no phase change, low energy consumption and low chemical sludge effluent [2–6].

Polyethersulfone (PES) is a well-known polymeric material which is widely employed in the nanofiltration (NF) membrane fabrication for numerous applications. Its unique characteristics include excellent chemical, mechanical and thermal resistance, soluble in aprotic organic solvent and relative resistance to heat aging making it ideal for asymmetric membrane preparation [7–9]. However, PES membrane is susceptible to membrane fouling during filtration

processes due to its inherited hydrophobic nature which in turn resulting severe flux decline, shortening membrane lifespan and maintenance cost increment [10]. Blending with hydrophilic additive has acquired much interest in order to change the PES membrane surface properties to be more hydrophilic due to their easy operation, high efficiency and lower cost. In particular, metal oxide particles (zinc oxide (ZnO) and titanium dioxide (TiO₂)) and carbon-based material (carbon nanotubes (CNTs) and graphene oxide (GO)) [8, 11–14] have been successfully mixed to the polymer matrix to improve membrane hydrophilicity and antifouling properties.

TiO₂ is known for its special properties such as commercial availability, low toxicity and chemical stability. Furthermore, its large surface area and unique self-cleaning behavior make them as a potential candidate material to be studied for wastewater treatment [11, 15]. Its capability to increase water permeability and antifouling properties has been recognized by many researchers since it is highly hydrophilic. Several reports have demonstrated that incorporation of TiO₂ could improve the membrane surface and fouling resistance. Guo and Kim [15] showed that hydrophilicity of the fabricated membrane measured by contact angle was improved from 68 to 57° for pristine PES and PES/TiO₂, respectively. PES/TiO₂ membrane also showed higher Bovine serum albumin rejection (99%) compared to that pristine PES membrane (96.5%). In addition, Ahmad et al. [11] agreed that TiO₂ can act as an excellent additive to enhance surface hydrophilicity and increased the membrane performance. They reported that the incorporation of 1 wt% of TiO₂ resulted a membrane with lower contact angle (67°) and higher water flux of 27.262 L/m²h compared with pristine PES membrane (72° and 21.196 L/m²h, respectively).

On the other hand, graphene oxide (GO) is also one of the promising materials to modify membrane surface properties. GO is a single layer of graphite oxide with one-atom layer thick. It has gained tremendous consideration in the membrane fabrication, and the research on its application value is still rising due to their distinctive properties. GO consists of abundance number of oxygen-functional groups (hydroxyl, carboxyl and epoxy groups) which make them highly hydrophilic [16]. As the consequence, GO can be easily dispersed into water or organic solvent [8, 17]. Alongside with these characteristics,

GO also known for its large surface area and excellent chemical stability. Many efforts have been done to develop a large-scale, high quality and purity of graphene production including electrochemical exfoliation method. Electrochemical exfoliation offers several benefits including one-step method, low cost, simple in operation and environmentally friendly since it can avoid harsh chemical consumption [18]. Through this method, GO can be exfoliated in ambient condition with the presence of an aqueous or non-aqueous electrolyte solution, graphite as an electrode and an electrical current.

GO-based membrane has been highlighted by many researchers, and its reports have been published for a long time [8, 16, 19–22]. In spite of its advantages, the GO agglomeration in polymer matrix is still inevitable which may result in poor membrane performance. Concerning this limitation, the utilization of surfactant for better GO dispersion in the polymer matrix is essentially needed. Previous work has reported that the triple-tail sodium 1,4-bis(neopentyl-oxo)-3-(neopentylcarbonyl)-1,4-dioxobutane-2-sulfonate (TC14) surfactant presented the highest CNTs dispersion as compared to the single- and double-tail surfactants [23]. In addition, a low GO agglomeration was obtained when the synthesized triple-tail TC14-based GO was intermixed with natural rubber latex [24]. The previous report has also showed that the utilization of triple-tail TC14 surfactant during GO synthesis has presented a smooth membrane surface and high dye rejection of 92.61% as compared to the single- and double-tail surfactants [21, 22].

In this work, the effect of different customized triple-tail surfactants' utilization; 1-butyl-3-methylimidazolium, 1, 4-bis(neopentyl-oxo)-3-(neopentyl-oxycarbonyl)-1, 4-dioxobutane-2-sulfonate (BMIM-TC14) and TC14 for better homogeneity and dispersion of GO sheet in polymer matrix has been investigated. It is believed that the utilization of these surfactants resulted in excellent performance of PES/GO-based membrane for wastewater treatment application. As far as it is known, the novelty of this study lies on the utilization of customized triple-tail BMIM-TC14 and TC14 surfactants for GO synthesis via electrochemical exfoliation and further utilized for methylene blue (MB) dye rejection application. This is the first attempt in comparing the effect of two different types of customized triple-tail surfactant on membrane morphology and performance. It has commonly been assumed that these surfactants'

utilization for PES/GO membrane fabrication will enhance membrane hydrophilicity, permeability, dye rejection and antifouling properties.

Materials and methods

Materials

Graphite rods (99.99% purity, 10 mm diameter and 150 mm length) obtained from GoodFellow GmbH, Germany were used as electrodes for GO synthesis. Other materials for GO synthesis include the customized triple-tail surfactants (BMIM-TC14 and TC14) and dimethylacetamide (DMAC) (Sigma-Aldrich) as solvent. The PES (grade in palette form) and commercial TiO₂ nanoparticles ($\geq 99.5\%$, Sigma-Aldrich) were used as the main polymer additive, respectively, to fabricate NF membrane. Meanwhile, the MB dye for dye rejection test was obtained from Sigma-Aldrich.

Graphene oxide synthesis

GO was synthesized via electrochemical exfoliation approach as reported by previous studies [21, 22, 25]. First, the customized triple-tail surfactants (BMIM-TC14 and TC14) were dissolved in DMAC solution to compose 0.1 M electrolyte solution. Two pieces of graphite rods were then partially immersed in the electrolyte solution followed by connecting to the 7 V DC power supply for 24 h.

PES/GO-based NF membrane preparation

PES/GO-based NF membrane was fabricated via non-solvent induced phase separation (NIPS) method. The casting solution consists of 20 wt% of PES and 1 wt% of TiO₂ which were dissolved in DMAC_GO_{BMIM-TC14} and DMAC_GO_{TC14} solution (79 wt%), respectively. On the other hand, pristine PES membrane was only dissolved into DMAC for comparison. Subsequently, the casting solution was stirred for 48 h at 70 °C until the homogenous solution was obtained. Thereafter, the well-mixed casting solution was placed at room temperature for overnight to ensure complete release of air bubbles before casting process. Once the casting solution had been prepared, the membrane was casted on a glass plate using a casting knife with 200 μm casting gap and then immersed in a deionised (DI) water for

overnight. After the initial phase separation, the fabricated membrane was kept in DI water until further measurements.

Membrane's characterizations

The surface and cross-sectional images of the fabricated NF membranes were observed via field emission scanning electron microscopy (FESEM) (Hitachi SU8020). Prior to analysis, to obtain a good membrane fracture for cross-sectional observation, the fabricated membranes were immersed in liquid nitrogen followed by coating with a gold layer to improve its conductivity. ImageJ software was also further used to confirm the pore size of the fabricated membranes. Meanwhile, energy-dispersive X-ray (EDX) instrument (Horiba EMAX) was performed to confirm the elemental composition of the fabricated NF membranes. The fabricated NF membranes' structural properties were then examined via micro-Raman spectroscopy (Renishaw InVia microRaman system) and X-ray diffraction (XRD) analysis (MiniFlex, Rigaku).

Nicolet 6700 Fourier transformed infrared spectroscopy (FTIR) analysis was performed to assess the fabricated NF membranes functionalities. Next, the surface morphology and roughness of the fabricated NF membranes were analyzed using atomic force micrograph (AFM) (Park System XE-100, Korea). Water contact angle measurement was then conducted using drop shape analysis (Optical Contact Angle 15EC, Dataphysics) to signify the membrane hydrophilicity. In brief, the dry membrane was placed on a glass slide and a droplet of water was dropped on the membrane surface followed by capturing the image.

Membrane porosity can be determined as the ratio of the membrane pores volume and its membrane total volume [5]. Therefore, to determine the membrane porosity, it was assumed that all the pores were completely filled with water. The gravimetric method was applied to determine the fabricated NF membranes porosity and further calculated using the following equation:

$$\varepsilon = \frac{(w_1 - w_2)/\rho_w}{[(w_1 - w_2)/\rho_w] + (w_2/\rho_p)} \times 100\% \quad (1)$$

where ε is membrane porosity (%), w_1 and w_2 are the wet and dry membrane weights (g), respectively, ρ_w is the water density (0.998 g/cm³) and ρ_p is the PES density (1.37 g/cm³).

The Sterlitech HP4750 dead-end cell system (effective membrane area 7.55 cm²) with a capacity of 200 mL was utilized to evaluate membrane permeation flux, dye rejection and antifouling properties of the fabricated NF membranes. Prior to permeation analysis, each membrane was pre-compacted with DI water at 0.6 MPa for 30 min to obtain a steady flux. Afterward, water flux measurement was conducted for 10 min by applying 5 different pressure levels (0.1–0.5 MPa). The water flux was then calculated using the following equation:

$$J = \frac{V}{A\Delta t} \quad (2)$$

where J is the permeated flux (L/m²h), V is the permeated water volume (m³), A is the membrane area (m²) and Δt is the permeation time (h).

In order to evaluate the fabricated NF membranes performance for dye rejection, 10 ppm concentration of MB dye solution was employed as feed solution. Then, it was followed by absorbance measurement of the treated dye solution by using UV–Vis spectroscopy. The dye rejection efficiency was then calculated using the following equation:

$$R(\%) = \left[1 - \frac{C_p}{C_o} \right] \times 100\% \quad (3)$$

where R is the dye rejection efficiency (%), C_p is the permeate dye concentration (ppm), and C_o is the initial dye concentration (ppm). After each dye rejection experiment, the fabricated NF membranes were thoroughly cleaned with DI water by pressuring the post-treated membrane for 30 min. Then, the water flux measurement of regenerated membrane was again evaluated at 0.2 MPa for 10 min. The flux recovery ratio (FRR) was calculated by the following formula:

$$\text{FRR} = \left[\frac{J_{w2}}{J_{w1}} \right] \times 100\% \quad (4)$$

where FRR is the flux recovery ratio, J_{w1} and J_{w2} are the initial water flux of the membrane before filtration process and water flux of the membrane after backwash process (membrane cleaning), respectively (L/m²h).

Results and discussion

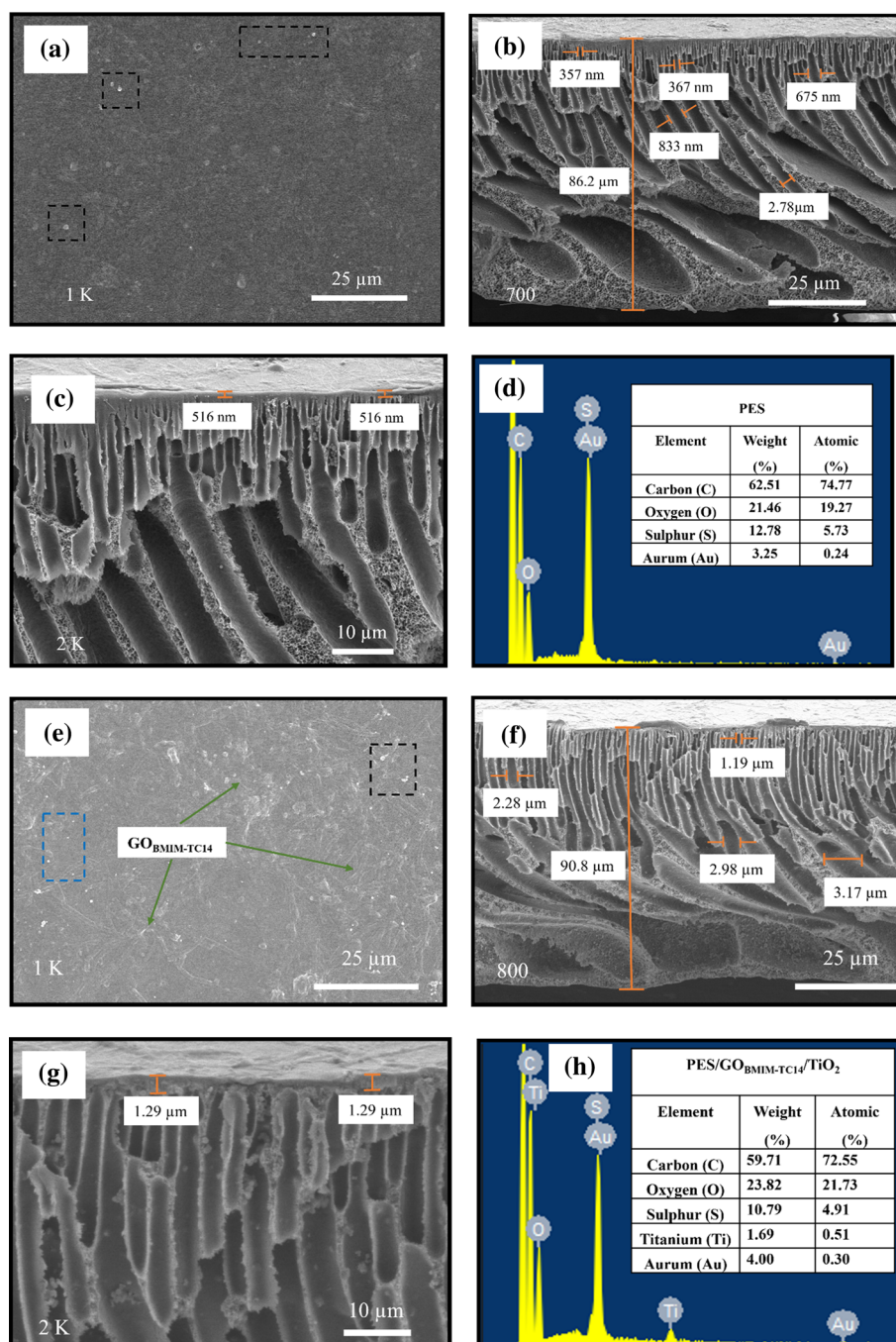
FESEM and EDX analysis

The surface and cross-sectional morphology of the fabricated NF membranes were examined via

FESEM, and the results are depicted in Fig. 1. Based on the surface morphology presented in Fig. 1a, e, and i, further measurement was carried out using an ImageJ software to confirm the fabricated membrane's pore size. Based on the measurement, all of the fabricated membranes presented a nanopore size, where the pristine PES, PES/GO_{BMIM-TC14}/TiO₂ and PES/GO_{TC14}/TiO₂ membranes pore size were 2.276, 2.673 and 4.343 nm, respectively. Therefore, it is confirmed that all of the fabricated membranes were NF membrane. Moreover, all of the fabricated membranes consist of asymmetric structure with finger-like structure. Still, the hybrid membrane had a different void structure as compared to pristine membrane. As could be seen from Fig. 1a, pristine PES membrane surface consists of smooth surface with small amount of nodule shapes on its surface (refer black rectangle shape), which indicated the presence of PES polymer [26]. For instance, the PES membrane presented short finger-like pores with the size ranged from 357 nm to 2.78 μm with thicker bottom layer lookalike sponge structure than the hybrid membrane (Fig. 1b). This morphology is frequently detected in PES membrane with additive-free [27, 28].

Meanwhile, the active layer thickness of PES membrane was found to be 516 nm as presented in Fig. 1c. EDX analysis in Fig. 1d then showed higher C atomic percentage of 74.77% over O and S element; 19.27 and 5.73%, respectively. The presence of S element was due to the sulfone and ether group of PES polymer. Next, as can be seen from Fig. 1 e and i, PES/GO_{BMIM-TC14}/TiO₂ and PES/GO_{TC14}/TiO₂ hybrid membranes exhibited smooth surface without any crack, thereby representing good surface durability of the fabricated NF membranes with GO and TiO₂ additives [29, 30]. Previous study reported that GO_{BMIM-TC14} presented a slightly better dispersion compared to GO_{TC14} due to the sodium counterions (Na⁺) replacement with imidazolium cations which simply affect the surfactant stability system [31]. Nevertheless, this study demonstrated that triple-tail TC14 resulted better exfoliation level of graphite and its stability in polymer matrix compared to triple-tail BMIM-TC14 when the electrolyte was replaced by DMAC. Consequently, higher GO content presence in PES/GO_{TC14}/TiO₂ membrane is observed as illustrated by its darker top surface than PES/GO_{BMIM-TC14}/TiO₂ membrane. In conclusion, the stabilizer and solvent choices have influenced the GO exfoliation degree and dispersion ability as well as

Figure 1 FESEM images of: **a–d** pristine PES, **e–h** PES/ $\text{GO}_{\text{BMIM-TC14}}/\text{TiO}_2$ and **i–l** PES/ $\text{GO}_{\text{TC14}}/\text{TiO}_2$ NF membranes.



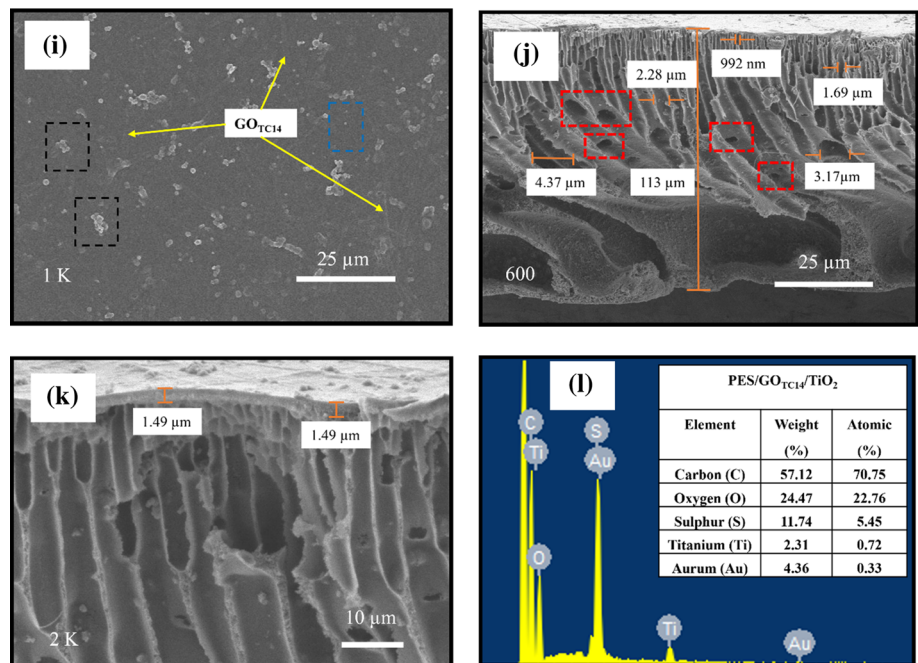
the dye rejection capability of the fabricated membrane.

In addition, it is interesting to consider the presence of nodules shape and white spot on both hybrid membrane's surfaces as well as on the cross-sectional images. Nevertheless, the nodules shape on the hybrid membrane's surface is uniform with no substantial defects. The presence of these nodules shape and white spot on both hybrid membrane's surfaces

could be corresponded to the PES polymer (black rectangle shape) and the entrapped TiO_2 particle (blue rectangle shape), respectively [11, 26]. Moreover, higher amount of nodule shape and white spot in PES/ $\text{GO}_{\text{TC14}}/\text{TiO}_2$ compared to the PES/ $\text{GO}_{\text{BMIM-TC14}}/\text{TiO}_2$ sample might be caused by the agglomeration of TiO_2 and PES polymer.

Considering Fig. 1f and j, there was no significant difference on the morphological properties of PES/

Figure 1 continued.



GO_{BMIM-TC14}/TiO₂ and PES/GO_{TC14}/TiO₂ sample. It can be seen from the cross-sectional images of the fabricated hybrid NF membrane, an asymmetric structure including dense-skin layer and porous finger-like structure as sublayer was observed in both samples. These skin layer played a pivotal role for the permeation and solute rejection, while porous sublayer enacts as mechanical support along with low resistance to water permeation [32, 33]. In the PES/GO_{BMIM-TC14}/TiO₂ and PES/GO_{TC14}/TiO₂ samples, the thickness of selective layer was found to be 1.29 (Fig. 1g) and 1.49 μm (Fig. 1k), respectively, thereby confirming that these two samples possessed higher selective layer thickness than pristine membrane (only 516 nm). Thicker selective layer of PES/GO_{TC14}/TiO₂ compared to PES/GO_{BMIM-TC14}/TiO₂ sample was believed attributed to the presence of higher GO content resulted from better exfoliation assisted by TC14 surfactant [34].

It is also known that the obtained membrane's structure is strongly related to the mechanisms of NIPS process. The introduction of hydrophilic additive in the membrane obviously alters the pore structures. In a general view, both of these membranes showed typical well-developed finger-like structure and spongy-like bottom support. As shown by the cross-sectional FESEM images, the finger-like structures become elongated and even extending toward the bottom region of both fabricated hybrid

NF membranes and its spongy-like bottom support almost unnoticeable. Besides, the pores of the interconnected support layer become close to each other and this kind of structure was believed to be a great help to assist membrane permeation.

Next, by comparing Fig. 1f and j, significant differences in the sublayer's structure can be observed. PES/GO_{TC14}/TiO₂ apparently showed longer finger-like structure with bulkier void structure at the bottom as compared to pristine PES and PES/GO_{BMIM-TC14}/TiO₂ membrane. In addition, the sizes of finger-like structure of PES/GO_{BMIM-TC14}/TiO₂ sample were in range of 1.19–3.17 μm, while PES/GO_{TC14}/TiO₂ sample was within range of 992 nm–437 μm, which was bigger than pristine PES. These results could be explained by the phenomenon of the accelerating solvent and non-solvent exchange rate induced by the GO in the phase inversion process [5, 35]. As one would expect, GO contained a large number of hydrophilic functional groups; therefore, blending the GO into the polymer matrix promotes the water diffusion from the coagulant bath to the membrane solution. In addition, during the phase inversion process, the macrovoid structure initially formed by the nucleation and grows in liquid–liquid phase separation [33]. Therefore, with the increase in the GO content, membrane solution become more hydrophilic which resulted in the faster diffusion of water into the polymer lean phases of the polymer

solution. This situation led to the big finger-like macrovoid formation in PES/GO_{TC14}/TiO₂ membrane [33].

In fact, the rapid exchange rate between the solvent and non-solvent during the membrane formation also affected the fabricated NF membrane thickness. Thicker PES/GO_{TC14}/TiO₂ sample (113 μm) in comparison with pristine PES (86.2 μm) (Fig. 1b) and PES/GO_{BMIM-TC14}/TiO₂ (90.8 μm) (Fig. 1f) is obviously observed (Fig. 1j). It is generally accepted that higher GO content promotes a rapid phase demixing during coagulation which then caused faster polymer chains precipitation and sequentially increased the membrane thickness [22, 36, 37]. Additionally, some transverse holes were observed in PES/GO_{TC14}/TiO₂ sublayer as highlighted by rectangle shape in Fig. 1j. The orientation of these holes was affected by the arbitrary of GO sheet in the polymer dopes. Since the GO was highly hydrophilic and PES/GO_{TC14}/TiO₂ membrane possess higher GO amount than PES/GO_{BMIM-TC14}/TiO₂ membrane, it promoted the water to surround GO sheet and form polymer lean phase.

As the water molecules flew along the GO surface, the orientation of microvoids formation in the sublayer was parallel to the GO surface [33]. Therefore, it is believed that hydrophilic nature and high amount of GO content resulted the transverse hole formation. Consequently, the water flux of the membrane may be affected since the original finger hole and the water flux communication may be interrupted with these transverse holes presence [33]. However, as being reported by Guo and Kim [15], this transverse orientation could also result in higher membrane permeability. Some structural and morphological similarities are in a good agreement with the previous reports [4, 15, 38, 39].

EDX analysis validates the existence of C, O, Ti, and S element in the fabricated hybrid NF membranes as depicted in Fig. 1h and i. PES/GO_{BMIM-TC14}/TiO₂ consists of C and O atomic percentage of 72.55 and 21.73%, respectively (Fig. 1h). Meanwhile, PES/GO_{TC14}/TiO₂ possessed lower and higher C (70.75%) and O (22.76%) content, respectively, as compared to PES/GO_{BMIM-TC14}/TiO₂ (Fig. 1i). Low Au atomic percentage (~ 0.30%) indicated the thin gold coating for FESEM analysis.

Further membrane's surface morphology investigation was performed using AFM, and the results are depicted in Fig. 2. Meanwhile, the obtained parameters including roughness average (R_a), root mean

square roughness (R_q) and average third highest peak to third lowest valley height (R_z) are summarized in Table 1. Generally, larger value of R_a , R_q and R_z indicated higher surface roughness [40]. As displayed by AFM images, the membrane roughness increases from 32.693 to 108.146 nm upon the addition of GO

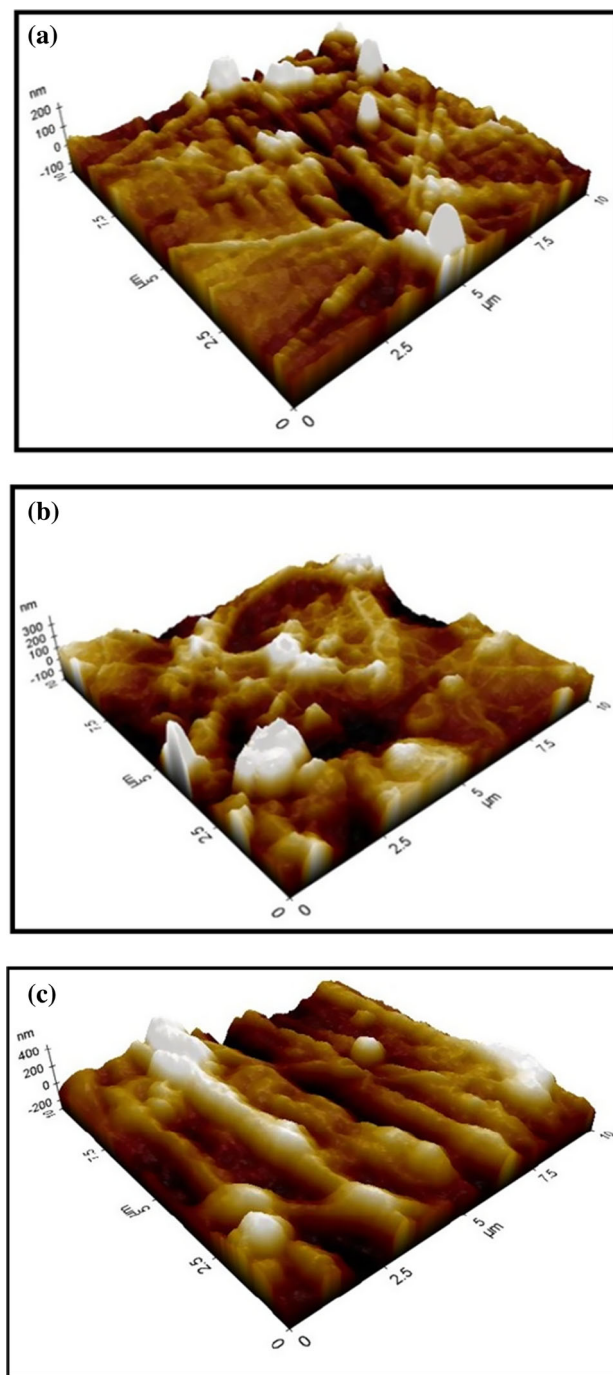


Figure 2 AFM images of: **a** pristine PES, **b** PES/GO_{BMIM-TC14}/TiO₂ and **c** PES/GO_{TC14}/TiO₂ NF membranes.

and TiO₂ as additives (see R_q values in Table 1). It is well known that the addition of hydrophilic GO and higher GO content could promote the top surface solidification rate which then can result in 1D shrinkage on the top surface of fabricated membrane once the casting solution was in contact with coagulating bath. This situation could lead to the spheres or nodules of polymer formation and causes the increase of the surface roughness [41]. There had been reported that the increase in surface roughness increases the effective membrane filtration area [42]. The increment in surface area and longer finger-like structure of PES/GO_{BMIM-TC14}/TiO₂ and PES/GO_{TC14}/TiO₂ membrane (as presented in FESEM images) are expected to improve the fluxes as compared to pristine PES.

Micro-Raman analysis

Figure 3 shows micro-Raman spectra of the fabricated NF membranes. Basically, Raman spectroscopy was applied to provide the significant insights regarding the quantitative chemical composition in the fabricated membrane. There are several peaks observed for pristine membrane that associated with PES in the range of 1000–1600 cm⁻¹ (Fig. 3a). The intense peak around 1148 cm⁻¹ associated with C–S (C–O) stretching mode of PES, while the other two peaks around 1072 and 1110 cm⁻¹ ascribed to the symmetric and asymmetric O=S=O groups stretching vibrations, respectively [43]. There also a peak at 1610 cm⁻¹ which correlated with in-plane benzene ring deformation [44].

Nevertheless, the PES peaks were unobserved for both hybrid membranes due to the weaker intensity peak of PES (Fig. 3b). Several peaks located at ~ 149, ~ 396, ~ 512 and ~ 638 cm⁻¹ proved the existence of TiO₂ as additive in the hybrid membrane matrixes. These peaks were matching to the TiO₂ anatase phase of E_g , B_{1g} , A_{1g} and E_g mode [21, 45].

Table 1 Surface roughness of the fabricated NF membranes based on AFM analysis

Membrane	R_a (nm)	R_q (nm)	R_z (nm)
PES	21.644	32.693	373.257
PES/GO _{BMIM-TC14} /TiO ₂	47.393	61.927	558.580
PES/GO _{TC14} /TiO ₂	81.001	108.146	758.501

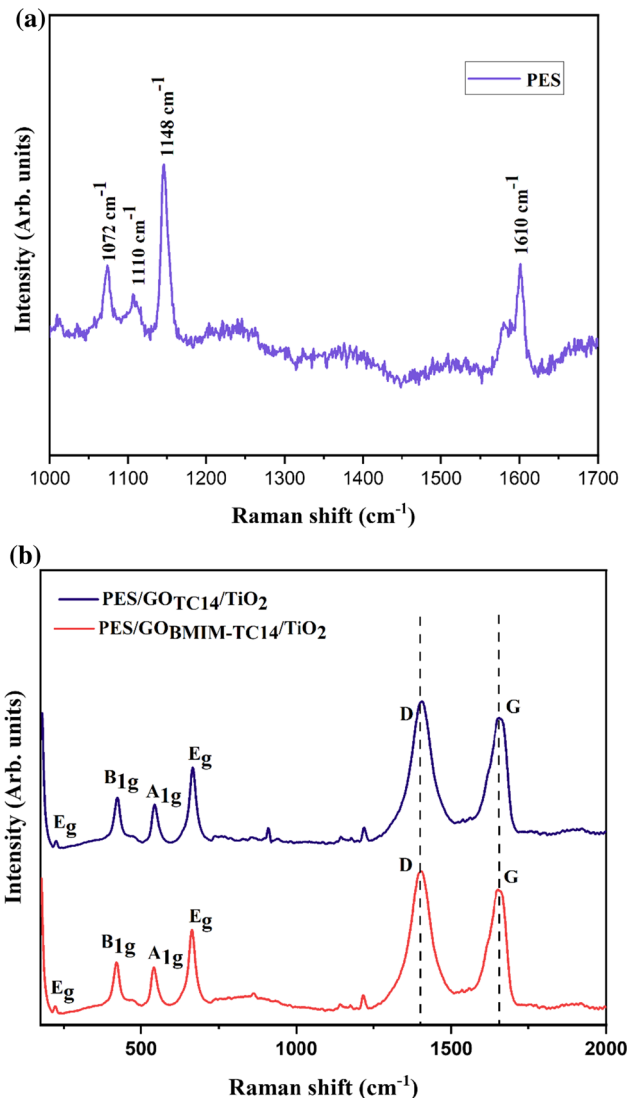


Figure 3 Micro-Raman Spectroscopy of the fabricated NF membranes: **a** Pristine PES, **b** PES/GO_{BMIM-TC14}/TiO₂ and PES/GO_{TC14}/TiO₂.

The presence of GO as additive also evidenced by two distinctive peaks (D- and G-band) observed in PES/GO_{BMIM-TC14}/TiO₂ and PES/GO_{TC14}/TiO₂ NF membranes. As depicted in Fig. 3b, it also can be seen that the D-band intensity of these hybrid membranes showed higher intensity than G-band, proved the successful exfoliation of graphite via electrochemical exfoliation method. D-band is related to the defects level in the graphite domain due to the presence of oxygen-containing functional group in the sample, while G-band is associated with the graphitic carbon in the structure.

The D- and G-band of PES/GO_{BMIM-TC14}/TiO₂ membrane was located at 1335.27 and 1569.61 cm⁻¹,

respectively. These peaks were shifted toward higher wavelength of 1337.03 and 1579.46 cm^{-1} , respectively, in PES/ $\text{GO}_{\text{TC14}}/\text{TiO}_2$ membrane. This result suggests that PES/ $\text{GO}_{\text{TC14}}/\text{TiO}_2$ membrane consists of fewer layer of exfoliated GO as compared to PES/ $\text{GO}_{\text{BMIM-TC14}}/\text{TiO}_2$ membrane [18]. In addition, the shifted peak between these two hybrid samples was believed due to a higher oxidation process promoted by TC14 surfactant during electrochemical exfoliation process [21].

Furthermore, the ratio between D- and G-band intensity ($I_{\text{D}}/I_{\text{G}}$) is related to the structural defect and often become a quality indicator to the produced material. It is believed that the ratio with high value showed higher defect density [18]. Based on calculation, PES/ $\text{GO}_{\text{TC14}}/\text{TiO}_2$ possessed higher $I_{\text{D}}/I_{\text{G}}$ ratio (1.04) compared to PES/ $\text{GO}_{\text{BMIM-TC14}}/\text{TiO}_2$ membrane (0.95), indicated that more defects exist in the PES/ $\text{GO}_{\text{TC14}}/\text{TiO}_2$ sample [46, 47]. This result then confirmed that the utilization of triple-tail TC14 surfactant during GO synthesis provided a better exfoliation of graphite and induce higher amount oxygen-containing functional group of GO than triple-tail BMIM-TC14 surfactant [21]. It is also believed that higher oxidation and exfoliation process may have enhanced the dye rejection and antifouling ability.

XRD analysis

Apart from its function to determine the changes in the material crystallinity, XRD analysis can also be used to spot the materials presence. Figure 4 depicts the XRD patterns of the fabricated NF membranes that clearly demonstrates a prominent diffraction peak without any crystallinity at $\sim 18^\circ$, thereby confirming the amorphous nature of PES polymer in all samples [48, 49]. After the incorporation of GO and TiO_2 in the sample, new peak formations were observed. In PES/ $\text{GO}_{\text{BMIM-TC14}}/\text{TiO}_2$ sample (Fig. 4b), the diffraction peaks of TiO_2 were distinguished at 25.06, 27.08, 37.3, 47.72, 53.76, 54.74 and 62.34° , which is consistent with the identified anatase phase peaks [50, 51]. Meanwhile, the pattern of anatase TiO_2 for PES/ $\text{GO}_{\text{TC14}}/\text{TiO}_2$ sample (Fig. 4c) showed the crystalline characteristic peak at 24.61, 25.72, 27.01, 37.08, 47.38, 53.34, 54.44 and 62.04° . Frequently, the incorporated additives may leach out of the polymer matrix due to their affinity with a non-solvent (water) [52]. However, the existence of TiO_2

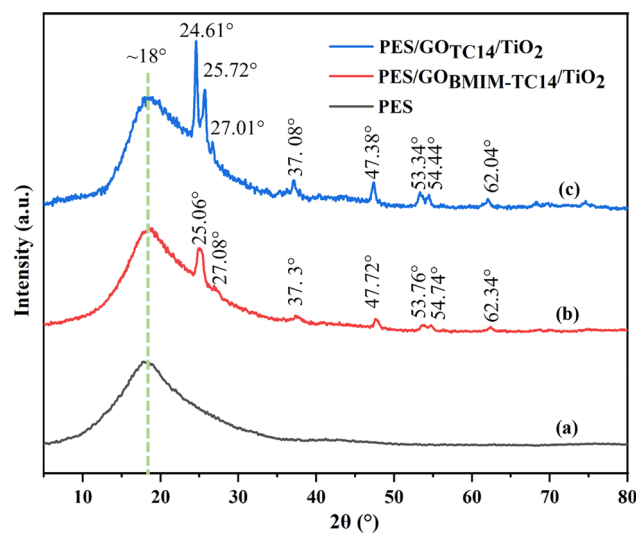


Figure 4 XRD analysis of the fabricated NF membranes: (a) Pristine PES, (b) PES/ $\text{GO}_{\text{BMIM-TC14}}/\text{TiO}_2$ and (c) PES/ $\text{GO}_{\text{TC14}}/\text{TiO}_2$.

peaks in both samples confirmed that the TiO_2 nanoparticles did not leach out from the dope solution during the process of phase inversion.

Nevertheless, the XRD analysis confirmed that the TiO_2 nanoparticles remained in the membrane matrix during the phase inversion process and have been distributed to the membrane [52, 53]. In addition, the crystalline peaks of TiO_2 for both hybrid samples exhibit a slight shift from typical TiO_2 peaks [54, 55], which was believed due to the interaction between PES and GO. However, it was notice that the diffraction peak of GO at $2\theta = \sim 10^\circ$ disappears in both of PES/ $\text{GO}_{\text{BMIM-TC14}}/\text{TiO}_2$ and PES/ $\text{GO}_{\text{TC14}}/\text{TiO}_2$ NF membranes. This might be due to the GO sheets regular stack that has been destroyed by TiO_2 intercalation [51, 55].

FTIR analysis

The chemical structure of the fabricated NF membranes was examined by FTIR analysis. The FTIR spectra of pristine PES, PES/ $\text{GO}_{\text{BMIM-TC14}}/\text{TiO}_2$ and PES/ $\text{GO}_{\text{TC14}}/\text{TiO}_2$ NF membranes are illustrated in Fig. 5. The aromatic ether ($-\text{C}-\text{O}-\text{C}-$) chemical bond of pristine PES, PES/ $\text{GO}_{\text{BMIM-TC14}}/\text{TiO}_2$ and PES/ $\text{GO}_{\text{TC14}}/\text{TiO}_2$ NF membranes can be found at 1011.87, 1012.27 and 1012.42 cm^{-1} , respectively [56]. Meanwhile, the peaks around 1153.20 and 1323.14 cm^{-1} appeared in the pristine PES membrane were caused by sulfone groups (SO_2) stretching

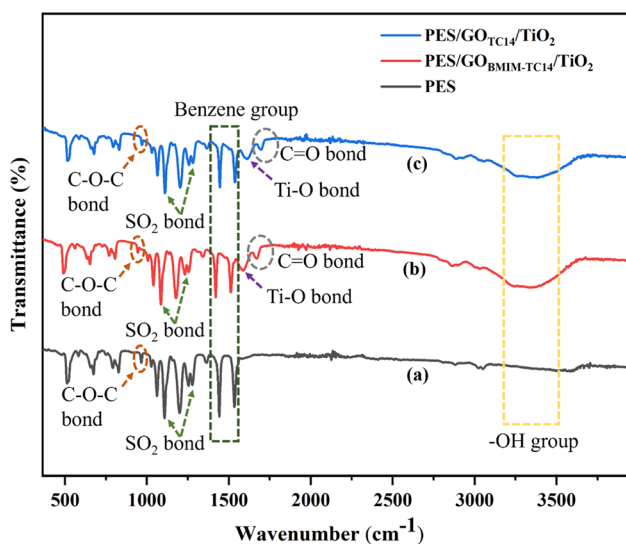


Figure 5 FTIR spectra of the fabricated NF membranes: (a) Pristine PES, (b) PES/GO_{BMIM-TC14}/TiO₂ and (c) PES/GO_{TC14}/TiO₂.

vibration [57]. However, these peaks were slightly shifted for both hybrid membranes; 1152.84 and 1322.76 cm⁻¹ for PES/GO_{BMIM-TC14}/TiO₂ and 1152.89 and 1322.81 cm⁻¹ for PES/GO_{TC14}/TiO₂ membrane. Lower wave number observed in both hybrid membranes was believed due to the formation of hydrogen bond between oxygen-functional group of GO and oxygen atom of the sulfone group. Meanwhile, C=O stretching vibration of PES/GO_{BMIM-TC14}/TiO₂ and PES/GO_{TC14}/TiO₂ membrane were located at 1737.88 and 1739.34 cm⁻¹, respectively [41]. Moreover, the backbone vibrations of benzene groups were also observed for pristine PES (1487.78 and 1579.65 cm⁻¹), PES/GO_{BMIM-TC14}/TiO₂ (1487.78 and 1579.35 cm⁻¹) and PES/GO_{TC14}/TiO₂ (1487.70 and 1579.37 cm⁻¹) membranes [56].

As demonstrated in Fig. 5b and c, two new formations of sharp peak at 1656.15 and 1653.06 cm⁻¹ were observed in both hybrid membranes that attributed to the Ti-O bond, thus confirmed the existence of TiO₂ as additive. In addition, a broad band at 3402.45 and 3427.86 cm⁻¹ associated with the stretching vibration of -OH group was also observed for PES/GO_{BMIM-TC14}/TiO₂ and PES/GO_{TC14}/TiO₂ NF membranes, respectively. However, due to the PES bonds interference, most of the peak related to the GO structure cannot be identified clearly in the FTIR spectra [58].

Hydrophilicity, contact angle and porosity analysis

The hydrophilicity of the fabricated membranes was determined by static contact angle measurement. Ordinarily, lower contact angle value indicated that the membrane surface exhibits higher hydrophilicity and better wettability to the water. As stated in Table 2, pristine PES membrane exhibited the highest contact angle value (77.35°) as compared to others fabricated membranes. This confirmed the high hydrophobic properties and poor wettability of PES membrane to water. In contrast, lower contact angle of PES/GO_{BMIM-TC14}/TiO₂ (70.99°) and PES/GO_{TC14}/TiO₂ (68.98°) membranes were observed and suggested an improved hydrophilicity of hybrid membranes.

As expected, the addition of GO and TiO₂ increased the membrane's hydrophilicity. The hydrophilic GO may migrate to the fabricated membrane surface during the demixing process then leading to the hydrophilicity increment. In addition, the highest hydrophilicity possessed by PES/GO_{TC14}/TiO₂ sample might be owed to the utilization of triple-tail TC14 surfactant during GO synthesis which provided a better exfoliation of graphite and induced higher amount of oxygen-functional group in GO_{TC14} solution as being demonstrated by higher I_D/I_G ratio of Raman analysis. In fact, PES/GO_{TC14}/TiO₂ may also contained more hydrogen bonds than other sample. Therefore, it was believed that hydrophilicity improvement of the hybrid membrane will affect membrane flux due to better attraction force between membrane surface and water droplet. Concurrently, antifouling ability was also expected to improve from the hydration layer presence on the membrane surface, i.e., higher flux recovery.

Furthermore, as clearly depicted in Table 2, the porosity measurement revealed an increment in the porosity as the incorporation of hydrophilic additives

Table 2 Contact angle and porosity measurement of the fabricated NF membranes

Membrane	Contact angle (°)	Porosity (%)
PES	77.35	88.40
PES/GO _{BMIM-TC14} /TiO ₂	70.99	90.14
PES/GO _{TC14} /TiO ₂	68.98	91.25

in the membrane matrix. For instance, the membrane porosity increased from $\sim 88\%$ (pristine PES) to ~ 90 and $\sim 91\%$ for PES/GO_{BMIM-TC14}/TiO₂ and PES/GO_{TC14}/TiO₂ membrane, respectively. This could be related to the functional group of GO and TiO₂ which rapidly promoted the diffusion of solvent molecules from the polymer matrix to the coagulation bath [27]. Therefore, higher porosity of PES/GO_{BMIM-TC14}/TiO₂ and PES/GO_{TC14}/TiO₂ membrane was obtained than those of pristine PES. The porosity values were in line with the FESEM observation, where PES/GO_{TC14}/TiO₂ showed more porous structure and presented lower contact angle value than those other membranes.

Water flux based on different operating pressure

The pure water flux and permeability are correlated with the fabricated membrane's hydrophilicity [27, 59]. In most cases, the water passage through membrane can be influenced by hydrophilicity, additional water channel provided by hydrophilic additives and the mean pore size of the fabricated membrane [59]. Figure 6 shows the pure water flux of the fabricated membranes at different applied pressures (0.1 to 0.5 MPa). As expected, the fluxes increased apparently by the trans-membrane pressure increment. Table 3 shows the pure water flux and water permeability of the fabricated pristine PES, PES/GO_{BMIM-TC14}/TiO₂ and PES/GO_{TC14}/TiO₂ membranes. It is well portrayed that upon the

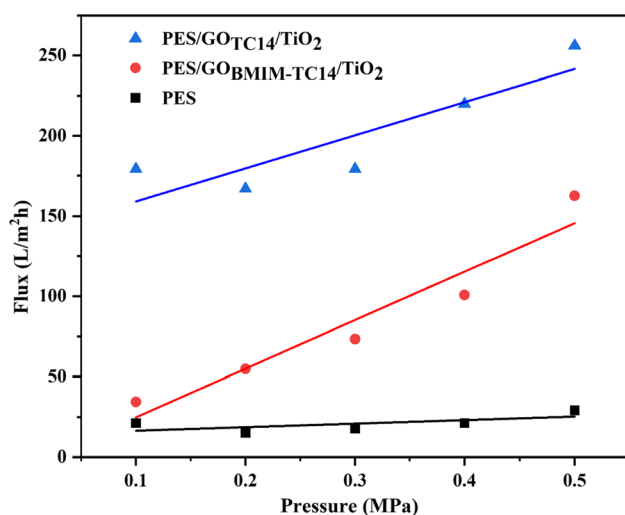


Figure 6 Water flux measurements of the fabricated NF membranes based on different level of driving pressure.

addition of hydrophilic GO and TiO₂, the pure water flux and permeability value significantly increased.

In fact, it was believed that the incorporation of triple-tail surfactant (BMIM-TC14 and TC14) provides an extra chain for GO and polymer interconnection with water molecules [21]. Generally, the hydrophobic nature of surfactant's tail is attached to the carbon bonds, while its hydrophilic head resides in the electrolyte solution. Therefore, the triple-tail surfactant is capable in providing triple interaction between GO layers and surfactant which further boost surfactant's intercalation into the GO inner layer spacing and resulted more stable GO sheets [24]. When these stable GO sheets were intermixed into polymer matrix, it is highly expected that better interaction between the polymer and GO was formed. This interaction will provide the triple pathway for water permeation through PVDF membrane thus resulted in higher water flux and permeability as the consequences.

Overall, the maximum pure water flux of the fabricated membrane was obtained to be 200.265 L/m²·h for PES/GO_{TC14}/TiO₂ membrane. Meanwhile, the lowest pure water flux was presented by PES membrane (20.839 L/m²·h) (see Table 3). In addition, PES/GO_{BMIM-TC14}/TiO₂ membrane presented fourfold increase in pure water flux (85.121 L/m²·h) than PES membrane, but still lower than PES/GO_{TC14}/TiO₂ membrane. This is consistent with the reported observation of their permeability, hydrophilicity and porosity. This confirmed that both hydrophilicity and porosity portrayed crucial contribution toward the membrane flux behavior. Furthermore, higher water flux and permeability of PES/GO_{BMIM-TC14}/TiO₂ and PES/GO_{TC14}/TiO₂ membranes compared to the pristine membrane could be attributed to the GO and TiO₂ presence [13]. Hydrophilic functional group contents providing additional spaces of water storage which further increases GO ability to attract water molecules. In addition, this also might be due to the size of water molecules itself, which are relatively small enough to pass freely through the GO nano-channels within the membrane surface [43]. On the hydrophilic surface, water droplet captivated onto membrane surface have greater surface energy that overpowers water surface tension. In consequence, this water droplet then passes smoothly into the hydrophilic pores, thus resulted a higher water flux [13].

Table 3 Dead-end filtration analysis on basis of pure water flux, water permeability, dye flux and rejection rate of the fabricated NF membranes

Membrane	Pure water flux (L/m ² ·h)	Water permeability (L/m ² ·h·MPa)	Dye flux (L/m ² ·h)	Rejection rate (%)
PES	20.839	9.142	3.311	87.67
PES/GO _{BMIM-TC14} /TiO ₂	85.121	28.780	29.801	86.14
PES/GO _{TC14} /TiO ₂	200.265	85.725	399.185	86.58

Dye rejection performance of the fabricated NF membrane

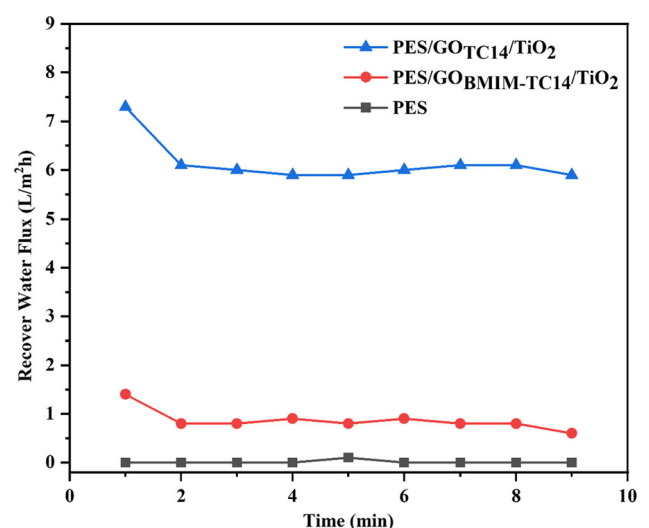
Generally, the rejection performance of pristine PES and the modified hybrid membranes are all found to be higher than 80% (Table 3). It appeared that the dye rejection efficiency (*R*) value of PES/GO_{TC14}/TiO₂ sample was slightly higher (86.58%) than that of PES/GO_{BMIM-TC14}/TiO₂ samples (86.14%). However, the pristine PES presented higher *R* value (87.67%) than hybrid membranes. Lower rejection rate of PES/GO_{TC14}/TiO₂ and PES/GO_{BMIM-TC14}/TiO₂ samples could be a result of the dye interaction with the composites, where positive charges of MB dye and its hydrophilic properties caused MB passing through the hydrophilic membrane surface [60]. Nevertheless, the rejection trend was reversely corresponded to the dye flux as the membrane with high rejection rate possessed low dye flux and vice versa. According to the dye flux measurement, PES/GO_{TC14}/TiO₂ sample exhibited the highest dye flux (399.185 L/m²·h), which was almost than four 100-fold and 13-fold higher than pristine PES (3.311 L/m²·h) and PES/GO_{BMIM-TC14}/TiO₂ (29.801 L/m²·h), respectively. This situation can be explained by its high hydrophilicity and porosity as compared to other membranes. In addition, the existence of higher hydrophilic groups on the PES/GO_{TC14}/TiO₂ surface plays a pivotal role in increasing dye flux. Hence, these finding leads to the conclusion that incorporation of triple-tail TC14 during GO synthesis offers better exfoliation thus affected the membrane performance.

Antifouling properties of the fabricated NF membrane

Membrane fouling occurred frequently and affected the membrane performance. During the filtration process, the foulant tends to be adsorbed on the membrane surface which then lead to the severe

fouling [9]. Antifouling property can be evaluated through membrane fouling evaluation. The results of antifouling experiments at the pressure of 0.2 MPa are illustrated in Fig. 7. The PES/GO_{TC14}/TiO₂ and PES/GO_{BMIM-TC14}/TiO₂ membranes flux decline was rapidly drop during the first 2 min before remain steady for the rest minute. Meanwhile, the flux decline curve of pristine PES was observed to be maintained from the first minute until the end. The slower flux decline claimed to be better antifouling property [61]. However, FRR value must take into consideration since it is the best index to describe antifouling property of the fabricated membrane.

Higher FRR value indicated that the fabricated membrane owns better antifouling property after easily swept away the foulant on its surface. As expected, PES/GO/TiO₂ membrane demonstrated high FRR compared to pristine PES membrane. The result revealed that pristine PES membrane only recovered the initial water flux value of about 5.88%. This might be due to an interaction between the

**Figure 7** Flux decline curve of the fabricated NF membranes measured at 0.2 MPa pressure.

foulant and hydrophobic surface of pristine PES membrane suggestive of irreversible fouling process [13]. In contrast, higher FRR value was noticed for the PES/GO_{BMIM-TC14}/TiO₂ (125.81%) and PES/GO_{TC14}/TiO₂ membrane (305.29%) owing to their higher hydrophilicity that portrayed a vital role in membrane fouling. It can be explained by higher membrane hydrophilicity which leading to the hydrophilic water layer formation on membrane surface. This water layer will act as protective layer and repels the foulant from attaching to the membrane surface [11, 27]. The antifouling properties improvement as discovered in this study was believed not only increase the lifespan of membrane but also can reduce cleaning cost and energy used for operation over time.

In addition, higher FRR value (> 100%) indicated that PES/GO/TiO₂ membrane was not only capable of restoring fouling, but at the same time, could retain additional flux after cleaning. This additional flux might be counteracted to the pore size enlargement after the filtration and cleaning process. This pattern has also been highlighted by several previous studies which discussed that the membrane pores size was increased as the filtration progressed [62, 63]. Marbelia et al. [63] reported that over each stage of filtration and maintenance cleaning, flux of the sample increased by more than 300% over time. They believed that the additive was slowly released over each stage of filtration and cleaning processes. Eventually, this situation might lead to a porosity increment (larger pore size). Therefore, we believed that higher FRR value of PES/GO/TiO₂ membrane might attribute to the additives that continue to leach out during the filtration or cleaning process, further leads to bigger pore size compared to the initial condition before the filtration process. This might explain the reason of higher FRR value of PES/GO_{TC14}/TiO₂ membrane since it already presented bigger pore size than that of pristine PES and PES/GO_{BMIM-TC14}/TiO₂ as being discussed in FESEM analysis (Fig. 1j). Therefore, pore size enlargement not only resulted in bigger pore size but also increases the membrane porosity.

Membrane fouling mechanism

Basically, membrane fouling can be caused by specific or nonspecific interactions between membrane surface and foulants. The specific interaction is

related to covalent bonding and coordination interaction formed between specific functional groups such as metal-carbonyl and amino-carbonyl. Meanwhile, nonspecific interaction attributed to the interaction of hydrogen bonding, hydrophobic, and electrostatic of the foulant and membrane surface. Figure 8 encapsulated the proposed fouling mechanism of the pristine PES and PES-based hybrid membrane. Generally, pore blocking due to the hydrophobic interaction is one of the factors that governed the membrane fouling for pristine membrane. When the hydrophilic organic or foulant with large molecular weight diffuse through the membrane, the tendency of these molecules to block the membrane passage is higher. At the moment of pristine PES making a contact with MB dye solution, the water molecule and membrane surface will resist to make a contact, and this situation is known as hydrophobic interaction [64]. This situation further resulted in direct contact of foulant particle and the membrane surface of pristine PES. The hydrophobic adsorption between membrane surface–foulants commonly leading to irreversible fouling. This may explain the poor antifouling properties of pristine PES since simple backwashing is not efficient in removing irreversible fouling [65].

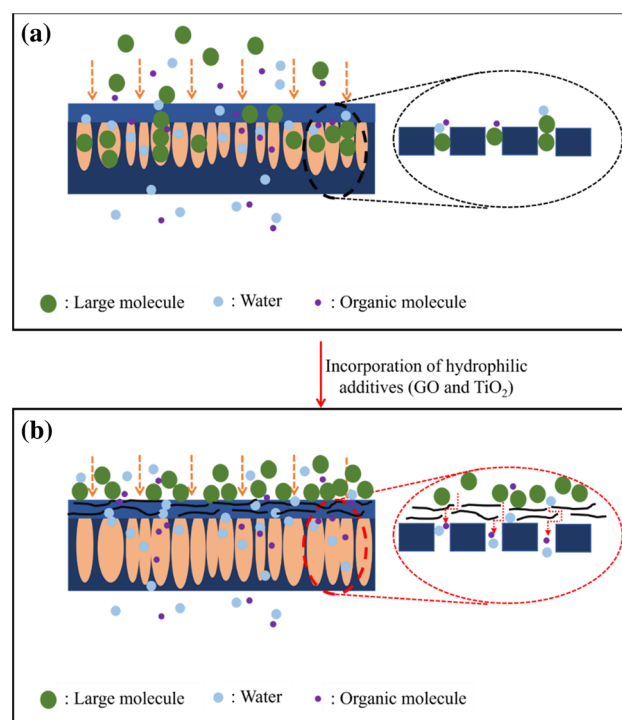


Figure 8 The proposed mechanism of membrane fouling for: **a** pristine PES and **b** PES/GO/TiO₂ hybrid membrane.

Table 4 Performance comparison of PES-based NF membrane with different additives

Additive	Water flux (L/ m ² h)	Dye flux ((L/ m ² h)	Rejection rate (%)	Reference
Tannic acid-coated boehmite (TA-BM)	111	–	Direct red 16: ~ 96	[4]
GO-ZnO	13.5	–	Trace organic compound: 75	[8]
Polyvinyl alcohol-Sodium alginate-GO	115.7	–	Lanasol blue 3R: 86.2	[27]
Dendrimer-polycitrate-alumoxane/polyvinyl pyrrolidone (PVP)	22.6	17.3	Direct red 16: 99	[66]
1, 3, 5-benzene-tricarbonyltri chloride (TMC), Pentaerythritol (PE)	6.1	–	Salt rejection (Na ₂ SO ₄): 98.1	[67]
Deep eutectic solvent/PVP	241.3	~ 100	Bovine serum albumin: 99	[68]
GO _{BMIM-TC14} -TiO ₂	85.121	29.801	MB: 86.14	This study
GO _{TC14} -TiO ₂	200.265	399.185	MB: 86.58	This study

With respect to the incorporation of hydrophilic additives; GO and TiO₂, the hydrophilicity of membrane could be enhanced by constructing the protective layers on membrane surface and increasing the network of hydrogen bonds of water. This protective layer can reduce the interaction force between the foulant and membrane surface, then leading to the prevention of irreversible foulant adsorption. The water molecules can easily pass through this protective layer since the hydrophilic additives tends to form hydrogen bond with water, further provided the path for them to pass through it. Nonetheless, the unwanted species or foulant were more prone to attach on the membrane surface and form a cake-layer. These cake-layer of foulant on the hybrid membrane surface owns a loose structure with weakened adhesion force. By using the simple cleaning or backwashing, these foulant can be easily removed from the membrane surface. Therefore, PES/GO/TiO₂ hybrid membrane displayed the better antifouling properties.

On the other hand, the membrane surface and foulant interaction might also include the electrostatic interaction. It could be either repulsive or attractive depending on the charges carried by the membrane and foulant. The foulant with the same charge of membrane surface will repel, while the opposite charge will promote the foulant adsorption on the surface. This interaction might occur in PES-based membrane. However, the zeta potential should be

further explored to obtain more accurate information before taking into consideration. For the moment, the main fouling mechanism for PES-based membrane might be hydrophobic interaction and hydrogen bonding rather than electrostatic interaction.

Comparative study of nanofiltration membrane

The fabricated PES/GO/TiO₂ membrane's effectiveness was then compared with identical class of NF membranes reported by other researchers to identify their performance, and the results are summarized in Table 4. It can be clearly seen that various additives have been employed to enhance PES membrane properties. However, none of these studies investigated PES membrane performance for MB dye rejection. In this study, two types of triple-tail surfactant (BMIM-TC14 and TC14) were also introduced to the PES/GO/TiO₂ membrane fabrication and its effect on morphological and rejection performance was studied. It should be note that the rejection rate of the fabricated membrane in this study might be lower than other researchers; however, the performance of the fabricated membranes was acceptable and its permeability was significantly improved compared to its pristine membrane and comparable to other previous works.

Conclusions

The PES-based membranes incorporated with hydrophilic additives were successfully fabricated via NIPS method employing customized triple-tail BMIM-TC14 and TC14 surfactants for GO synthesis by electrochemical exfoliation method. The influence of triple-tail surfactant on the membrane capability and fouling endurance was elucidated with emphasis on pure water flux, MB dye rejection and FRR value. Based on the obtained results, it was found that triple-tail TC14 surfactant resulted the highest membrane's porosity (91.296%) and hydrophilicity as indicated by the lowest contact angle value (68.98°) as compared to all fabricated membranes. In addition, higher dye flux (399.185 L/m²·h) and dye rejection (86.58%) was presented by PES/GO_{TC14}/TiO₂ NF membrane. Besides, its higher FRR value (305.29%) confirming that PES/GO_{TC14}/TiO₂ NF membrane owns acceptable antifouling ability. Overall, the acquired results proposed that the incorporation of particular GO and TiO₂ as hydrophilic additives had major influence to boost membrane performance and antifouling ability.

Acknowledgements

The authors acknowledge the financial support from the Fundamental Research Grand Scheme (grant no. 2020-0254-103-02) and Newton Fund: Use of ISIS Neutron and Muon Source (grant no. 2019-0257-103-11).

Data availability

Not applicable.

Declarations

Conflicts of interest The authors have no conflict of interest to declare.

References

- [1] Van TTT, Kumar SR, Lue SJ (2019) Separation mechanisms of binary dye mixtures using a PVDF ultrafiltration membrane: donnan effect and intermolecular interaction. *J Memb Sci* 575:38–49. <https://doi.org/10.1016/j.memsci.2018.12.070>
- [2] Kim BS, Lee J (2016) Macroporous PVDF/TiO₂ membranes with three-dimensionally interconnected pore structures produced by directional melt crystallization. *Chem Eng J* 301:158–165. <https://doi.org/10.1016/j.cej.2016.05.003>
- [3] Nasrollahi N, Ghalamchi L, Vatanpour V, Khataee A (2021) Photocatalytic-membrane technology: a critical review for membrane fouling mitigation. *J Ind Eng Chem* 93:101–116. <https://doi.org/10.1016/j.jiec.2020.09.031>
- [4] Oulad F, Zinadini S, Akbar A, Ashraf A (2020) Fabrication and characterization of a novel tannic acid coated boehmite/PES high performance antifouling NF membrane and application for licorice dye removal. *Chem Eng J* 397:125105. <https://doi.org/10.1016/j.cej.2020.125105>
- [5] Xia S, Ni M (2014) Preparation of poly(vinylidene fluoride) membranes with graphene oxide addition for natural organic matter removal. *J Memb Sci* 473:54–62. <https://doi.org/10.1016/j.memsci.2014.09.018>
- [6] Wang K, Qin Y, Quan S et al (2019) Development of highly permeable polyelectrolytes (PEs)/UiO-66 nanofiltration membranes for dye removal. *Chem Eng Res Des* 147:222–231. <https://doi.org/10.1016/j.cherd.2019.05.014>
- [7] Dehban A, Kargari A, Ashtiani FZ (2020) Preparation and optimization of antifouling PPSU/PES/SiO₂ nanocomposite ultrafiltration membranes by VIPS-NIPS technique. *J Ind Eng Chem* 88:292–311. <https://doi.org/10.1016/j.jiec.2020.04.028>
- [8] Mahlangu OT, Nackaerts R, Thwala JM et al (2017) Hydrophilic fouling-resistant GO-ZnO/PES membranes for wastewater reclamation. *J Memb Sci* 524:43–55. <https://doi.org/10.1016/j.memsci.2016.11.018>
- [9] Ma J, Guo X, Ying Y et al (2017) Composite ultrafiltration membrane tailored by MOF@GO with highly improved water purification performance. *Chem Eng J* 313:890–898. <https://doi.org/10.1016/j.cej.2016.10.127>
- [10] Matindi CN, Hu M, Kadanyo S et al (2021) Tailoring the morphology of polyethersulfone/sulfonated polysulfone ultrafiltration membranes for highly efficient separation of oil-in-water emulsions using TiO₂ nanoparticles. *J Memb Sci* 620:118868. <https://doi.org/10.1016/j.memsci.2020.118868>
- [11] Ahmad AL, Pang WY, Mohd Shafie ZMH, Zaulkiflee ND (2019) PES/PVP/TiO₂ mixed matrix hollow fiber membrane with antifouling properties for humic acid removal. *J Water Process Eng* 31:1–9. <https://doi.org/10.1016/j.jwpe.2019.100827>
- [12] Algamdi MS, Alsohaimi IH, Lawler J et al (2019) Fabrication of graphene oxide incorporated polyethersulfone hybrid ultrafiltration membranes for humic acid removal. *Sep Purif*

- Technol 223:17–23. <https://doi.org/10.1016/j.seppur.2019.04.057>
- [13] Makhetha TA, Moutloali RM (2021) Incorporation of a novel Ag – Cu@ZIF-8@GO nanocomposite into polyethersulfone membrane for fouling and bacterial resistance. *J Memb Sci* 618:118733. <https://doi.org/10.1016/j.memsci.2020.118733>
- [14] Shahrudin MZ, Zakaria N, Diana Junaidi NF et al (2017) Study of the effectiveness of Titanium Dioxide (TiO₂) nanoparticle in Polyethersulfone (PES) Composite membrane for removal of oil in oily wastewater. *J Appl Membr Sci Technol* 19:33–42. <https://doi.org/10.1111/amst.v19i1.21>
- [15] Guo J, Kim J (2017) Modifications of polyethersulfone membrane by doping sulfated-TiO₂ nanoparticles for improving anti-fouling property in wastewater treatment. *RSC Adv* 7:33822–33828. <https://doi.org/10.1039/c7ra06406c>
- [16] Zhao G, Hu R, Zhao X et al (2019) High flux nanofiltration membranes prepared with a graphene oxide homo-structure. *J Memb Sci* 585:29–37. <https://doi.org/10.1016/j.memsci.2019.05.028>
- [17] Ray SC (2015) Application and uses of Graphene oxide and reduced Graphene oxide. *Appl Graphene Graphene-Oxide Based Nanomater*. <https://doi.org/10.1016/b978-0-323-37521-4.00002-9>
- [18] Konstantopoulos G, Fotou E, Ntziouni A et al (2021) A systematic study of electrolyte effect on exfoliation efficiency and green synthesis of graphene oxide. *Ceram Int* 47:32276–32289. <https://doi.org/10.1016/j.ceramint.2021.08.122>
- [19] Bagheripour E, Moghadassi AR, Hosseini SM et al (2018) Novel composite graphene oxide/chitosan nanoplates incorporated into PES based nanofiltration membrane: chromium removal and antifouling enhancement. *J Ind Eng Chem* 62:311–320. <https://doi.org/10.1016/j.jiec.2018.01.009>
- [20] Chen C, Yang QH, Yang Y et al (2009) Self-assembled free-standing graphite oxide membrane. *Adv Mater* 21:3007–3011. <https://doi.org/10.1002/adma.200803726>
- [21] Mohamat R, Suriani AB, Mohamed A et al (2021) Effect of Surfactants' tail number on the PVDF/GO/TiO₂-Based Nanofiltration membrane for dye rejection and antifouling performance improvement. *Int J Environ Res* 15:149–161. <https://doi.org/10.1007/s41742-020-00299-6>
- [22] Suriani AB, Muqoyyanah Mohamed A et al (2019) Incorporation of electrochemically exfoliated graphene oxide and TiO₂ into polyvinylidene fluoride-based nanofiltration membrane for dye rejection. *Water Air Soil Pollut* 230:176. <https://doi.org/10.1007/s11270-019-4222-x>
- [23] Mohamed A, Anas AK, Abu Bakar S et al (2014) Preparation of multiwall carbon nanotubes (MWCNTs) stabilised by highly branched hydrocarbon surfactants and dispersed in natural rubber latex nanocomposites. *Colloid Polym Sci* 292:3013–3023. <https://doi.org/10.1007/s00396-014-3354-1>
- [24] Suriani AB, Nurhafizah MD, Mohamed A et al (2016) Highly conductive electrodes of graphene oxide/natural rubber latex-based electrodes by using a hyper-branched surfactant. *JMADE*. <https://doi.org/10.1016/j.matdes.2016.03.067>
- [25] Suriani AB, Muqoyyanah MA et al (2018) Reduced graphene oxide-multiwalled carbon nanotubes hybrid film with low Pt loading as counter electrode for improved photovoltaic performance of dye-sensitised solar cells. *J Mater Sci Mater Electron* 29:10723–10743. <https://doi.org/10.1007/s10854-018-9139-4>
- [26] Rahimpour A, Madaeni SS, Amirinejad M et al (2009) The effect of heat treatment of PES and PVDF ultrafiltration membranes on morphology and performance for milk filtration. *J Memb Sci* 330:189–204. <https://doi.org/10.1016/j.memsci.2008.12.059>
- [27] Amiri S, Asghari A, Vatanpour V, Rajabi M (2020) Fabrication and characterization of a novel polyvinyl alcohol-graphene oxide-sodium alginate nanocomposite hydrogel blended PES nano filtration membrane for improved water purification. *Sep Purif Technol* 250:117216. <https://doi.org/10.1016/j.seppur.2020.117216>
- [28] Ocakoglu K, Dizge N, Colak SG et al (2021) Polyethersulfone membranes modified with CZTS nanoparticles for protein and dye separation: Improvement of antifouling and self-cleaning performance. *Colloids Surfaces A Physicochem Eng Asp* 616:126230. <https://doi.org/10.1016/j.colsurfa.2021.126230>
- [29] Karimipour H, Shahbazi A, Vatanpour V (2021) Fouling decline and retention increase of polyethersulfone membrane by incorporating melamine-based dendrimer amine functionalized graphene oxide nanosheets (GO/MDA). *J Environ Chem Eng* 9:104849. <https://doi.org/10.1016/j.jece.2020.104849>
- [30] Safarpour M, Vatanpour V, Khataee A (2016) Preparation and characterization of graphene oxide/TiO₂ blended PES nanofiltration membrane with improved antifouling and separation performance. *Desalination* 393:65–78. <https://doi.org/10.1016/j.desal.2015.07.003>
- [31] Mohamed A, Ardyani T, Bakar SA et al (2018) Preparation of conductive cellulose paper through electrochemical exfoliation of graphite: the role of anionic surfactant ionic liquids as exfoliating and stabilizing agents. *Carbohydr Polym* 201:48–59. <https://doi.org/10.1016/j.carbpol.2018.08.040>

- [32] Wang J, Lang WZ, Xu HP et al (2015) Improved poly(vinyl butyral) hollow fiber membranes by embedding multi-walled carbon nanotube for the ultrafiltrations of bovine serum albumin and humic acid. *Chem Eng J* 260:90–98. <https://doi.org/10.1016/j.cej.2014.08.082>
- [33] Yang M, Zhao C, Zhang S et al (2017) Preparation of graphene oxide modified poly(m-phenylene isophthalamide) nanofiltration membrane with improved water flux and antifouling property. *Appl Surf Sci* 394:149–159. <https://doi.org/10.1016/j.apsusc.2016.10.069>
- [34] Wang J, Wang Y, Zhu J et al (2017) Construction of TiO₂@graphene oxide incorporated antifouling nanofiltration membrane with elevated filtration performance. *J Memb Sci* 533:279–288. <https://doi.org/10.1016/j.memsci.2017.03.040>
- [35] Wu L, Zhang X, Wang T et al (2019) Enhanced performance of polyvinylidene fluoride ultrafiltration membranes by incorporating TiO₂/graphene oxide. *Chem Eng Res Des* 141:492–501. <https://doi.org/10.1016/j.cherd.2018.11.025>
- [36] Esmaili M, Lahti J, Virtanen T et al (2020) The interplay role of vanillin, water, and coagulation bath temperature on formation of antifouling polyethersulfone (PES) membranes: application in wood extract treatment. *Sep Purif Technol* 235:116225. <https://doi.org/10.1016/j.seppur.2019.116225>
- [37] Nikooe N, Saljoughi E (2017) Preparation and characterization of novel PVDF nanofiltration membranes with hydrophilic property for filtration of dye aqueous solution. *Appl Surf Sci* 413:41–49. <https://doi.org/10.1016/j.apsusc.2017.04.029>
- [38] Vatanpour V, Madaeni SS, Khataee AR et al (2012) TiO₂ embedded mixed matrix PES nanocomposite membranes: influence of different sizes and types of nanoparticles on antifouling and performance. *Desalination* 292:19–29. <https://doi.org/10.1016/j.desal.2012.02.006>
- [39] Jiang B, Zhang N, Zhang L et al (2018) Enhanced separation performance of PES ultrafiltration membranes by imidazole-based deep eutectic solvents as novel functional additives. *J Memb Sci* 564:247–258. <https://doi.org/10.1016/j.memsci.2018.07.034>
- [40] Balkanloo PG, Mahmoudian M, Hosseinzadeh MT (2020) A comparative study between MMT-Fe₃O₄/PES, MMT-HBE/PES, and MMT-acid activated/PES mixed matrix membranes. *Chem Eng J* 396:125188. <https://doi.org/10.1016/j.cej.2020.125188>
- [41] Chu Z, Chen K, Xiao C et al (2020) Performance improvement of polyethersulfone ultrafiltration membrane containing variform inorganic nano-additives. *Polymer (Guildf)* 188:122160. <https://doi.org/10.1016/j.polymer.2020.122160>
- [42] Mahmoudi E, Yong L, Lun W et al (2020) Improving membrane bioreactor performance through the synergistic effect of silver-decorated graphene oxide in composite membranes. *J Water Process Eng* 34:101169. <https://doi.org/10.1016/j.jwpe.2020.101169>
- [43] Ly QV, Matindi C, Kuvarega AT et al (2020) Exploring the novel PES/malachite mixed matrix membrane to remove organic matter for water purification. *Chem Eng Res Des* 160:63–73. <https://doi.org/10.1016/j.cherd.2020.05.022>
- [44] Ahmad MW, Dey B, Al Saidi AKA, Choudhury A (2020) Functionalized-graphene reinforced polyethersulfone nanocomposites with improved physical and mechanical properties. *Polym Compos* 41:4104–4116. <https://doi.org/10.1002/pc.25697>
- [45] Kumi-Barimah E, Penhale-Jones R, Salimian A et al (2020) Phase evolution, morphological, optical and electrical properties of femtosecond pulsed laser deposited TiO₂ thin films. *Sci Rep* 10:1–12. <https://doi.org/10.1038/s41598-020-67367-x>
- [46] Francolini I, Perugini E, Silvestro I et al (2019) Graphene oxide oxygen content affects physical and biological properties of scaffolds based on chitosan/graphene oxide conjugates. *Materials (Basel)* 12:1142–1158. <https://doi.org/10.3390/ma12071142>
- [47] Khan U, O'Neill A, Lotya M et al (2010) High-concentration solvent exfoliation of graphene. *Small* 6:864–871. <https://doi.org/10.1002/sml.200902066>
- [48] Kazemi M, Peyravi M, Jahanshahi M (2020) Multilayer UF membrane assisted by photocatalytic NZVI@TiO₂ nanoparticle for removal and reduction of hexavalent chromium. *J Water Process Eng* 37:101183. <https://doi.org/10.1016/j.jwpe.2020.101183>
- [49] Abdulkarem E, Ibrahim Y, Naddeo V et al (2020) Development of Polyethersulfone/ α -Zirconium phosphate (PES/ α -ZrP) flat-sheet nanocomposite ultrafiltration membranes. *Chem Eng Res Des* 161:206–217. <https://doi.org/10.1016/j.cherd.2020.07.006>
- [50] Khalid F, Tabish M, Bora KAI (2020) Novel poly(vinyl alcohol) nanofiltration membrane modified with dopamine coated anatase TiO₂ core shell nanoparticles. *J Water Process Eng* 37:101486. <https://doi.org/10.1016/j.jwpe.2020.101486>
- [51] Li C, Sun W, Lu Z et al (2019) Systematic evaluation of TiO₂-GO-modified ceramic membranes for water treatment: retention properties and fouling mechanisms. *Chem Eng J* 378:122138. <https://doi.org/10.1016/j.cej.2019.122138>
- [52] Kusworo TD, Ariyanti N, Utomo DP (2020) Effect of nano-TiO₂ loading in polysulfone membranes on the removal of pollutant following natural-rubber wastewater treatment. *J Water Process Eng* 35:101190. <https://doi.org/10.1016/j.jwpe.2020.101190>

- [53] Wu G, Gan S, Cui L, Xu Y (2008) Preparation and characterization of PES/TiO₂ composite membranes. *Appl Surf Sci* 254:7080–7086. <https://doi.org/10.1016/j.apsusc.2008.05.221>
- [54] Jaleh B, Zare E, Azizian S et al (2020) Preparation and characterization of polyvinylpyrrolidone/polysulfone ultrafiltration membrane modified by graphene oxide and titanium dioxide for enhancing hydrophilicity and antifouling properties. *J Inorg Organomet Polym Mater* 30:2213–2223. <https://doi.org/10.1007/s10904-019-01367-x>
- [55] Zhang H, Wang X, Li N et al (2018) Synthesis and characterization of TiO₂/graphene oxide nanocomposites for photoreduction of heavy metal ions in reverse osmosis concentrate. *RSC Adv* 8:34241–34251. <https://doi.org/10.1039/c8ra06681g>
- [56] Farnam M, Mukhtar H, Shariff AM (2016) An investigation of blended polymeric membranes and their gas separation performance. *RSC Adv* 6:102671–102679. <https://doi.org/10.1039/c6ra21574b>
- [57] Li YN, Li H, Ye H et al (2019) Preparation and characterization of poly(ether sulfone)/fluorinated silica organic–inorganic composite membrane for sulfur dioxide desulfurization. *High Perform Polym* 31:72–85. <https://doi.org/10.1177/0954008317752072>
- [58] Alkindy MB, Naddeo V, Banat F, Hasan SW (2020) Synthesis of polyethersulfone (PES)/GO-SiO₂ mixed matrix membranes for oily wastewater treatment. *Water Sci Technol* 81:1354–1364. <https://doi.org/10.2166/wst.2019.347>
- [59] Giwa A, Hasan SW (2020) Novel polyethersulfone-functionalized graphene oxide (PES-fGO) mixed matrix membranes for wastewater treatment. *Sep Purif Technol* 241:116735. <https://doi.org/10.1016/j.seppur.2020.116735>
- [60] Makhetha TA, Moutloali RM (2018) Antifouling properties of Cu (tpa)@GO/PES composite membranes and selective dye rejection. *J Memb Sci* 554:195–210. <https://doi.org/10.1016/j.memsci.2018.03.003>
- [61] Zhu Z, Wang L, Xu Y et al (2017) Preparation and characteristics of graphene oxide-blending PVDF nanohybrid membranes and their applications for hazardous dye adsorption and rejection. *J Colloid Interface Sci* 504:429–439. <https://doi.org/10.1016/j.jcis.2017.05.068>
- [62] Ambarita AC, Mulyati S, Arahman N et al (2021) Improvement of properties and performances of polyethersulfone ultrafiltration membrane by blending with bio-based dragonbloodin resin. *Polymers (Basel)*. <https://doi.org/10.3390/polym13244436>
- [63] Marbelia L, Bilad MR, Vankelecom IFJ (2019) Gradual PVP leaching from PVDF/PVP blend membranes and its effects on membrane fouling in membrane bioreactors. *Sep Purif Technol* 213:276–282. <https://doi.org/10.1016/j.seppur.2018.12.045>
- [64] Xu H, Xiao K, Wang X et al (2020) Outlining the roles of membrane-Foulant and Foulant-Foulant interactions in organic fouling during microfiltration and ultrafiltration: a mini-review. *Front Chem* 8:1–14. <https://doi.org/10.3389/fchem.2020.00417>
- [65] Gao Y, Qin J, Wang Z, Østerhus SW (2019) Backpulsing technology applied in MF and UF processes for membrane fouling mitigation: a review. *J Memb Sci* 587:117136. <https://doi.org/10.1016/j.memsci.2019.05.060>
- [66] Zinadini S, Gholami F (2016) Preparation and characterization of high flux PES nanofiltration membrane using hydrophilic nanoparticles by phase inversion method for application in advanced wastewater treatment. *J Appl Res Water Wastewater* 5:232–235
- [67] Cheng J, Shi W, Zhang L, Zhang R (2017) A novel polyester composite nanofiltration membrane formed by interfacial polymerization of pentaerythritol (PE) and trimesoyl chloride (TMC). *Appl Surf Sci* 416:152–159. <https://doi.org/10.1016/j.apsusc.2017.04.173>
- [68] Vatanpour V, Dehqan A, Harifi-Mood AR (2020) Ethaline deep eutectic solvent as a hydrophilic additive in modification of polyethersulfone membrane for antifouling and separation improvement. *J Memb Sci* 614:118528. <https://doi.org/10.1016/j.memsci.2020.118528>

Publisher's Note Springer Nature remains neutral with regard to jurisdictional claims in published maps and institutional affiliations.

Springer Nature or its licensor holds exclusive rights to this article under a publishing agreement with the author(s) or other rightsholder(s); author self-archiving of the accepted manuscript version of this article is solely governed by the terms of such publishing agreement and applicable law.